Links between mesopause temperatures and ground-based VLF narrowband radio signals

Israel Silber[1], Colin Price[1], Craig J. Rodger[2] and Christos Haldoupis[3]

[1]Department of Geophysical, Atmospheric and Planetary Sciences

Tel Aviv University, Israel

[2]Department of Physics, University of Otago, New Zealand

[3]Physics Department, University of Crete, Greece

January, 2013

Abstract

The Upper Mesosphere-Lower Thermosphere (UMLT) region of the atmosphere is known to vary on many temporal and spatial scales. However, this region of the atmosphere is very difficult to measure and monitor continuously. In this paper we demonstrate an intriguing connection between mesopause temperatures and the intensity of Very Low Frequencies (VLF) narrowband (NB) signals reflected off the lower ionosphere. The temperature data used are from the SABER instrument on-board the TIMED satellite, while the VLF data are obtained from various ground-based receiving systems. The results of the analysis show a high anti-correlation between temperature and VLF amplitude. It is shown that the variability of the UMLT temperatures and VLF amplitudes can be explained by global seasonal solar irradiance changes (~72% of the variability), while the remaining variability has its origins from other sources (~28%). High resolution mesopause temperature estimates might be achieved in the future by combining VLF NB observations and calculated solar irradiance variability (as a function of hour, day, and location, i.e., latitude).

1. Introduction

The mesopause region of the Earth's atmosphere, which is sometimes referred to as the Upper Mesosphere-Lower Thermosphere (UMLT) region, is the layer between the mesosphere and the thermosphere, lying between 80 km (summer) and 100 km (winter) altitude [Havnes et al., 1990; Yu and She, 1995; Ortland et al., 1998; Smith, 2004; Bittner et al., 2010], and represents the coldest region of the atmosphere. This region of the atmosphere is also part of the D and E layers of the ionosphere, the electrified part of the atmosphere [Kamide and Chian, 2007].

The mesopause region's height, temperature, and thickness, together with the electrical conductivity of this part of the ionosphere are known to vary on different spatial and temporal scales, from local up to global scale, and from temporal scales of seconds up to periods of years. Some of these variations are transient, created by phenomena such as gravity waves, infrasound, and geomagnetic disturbances [e.g., Bittner et al., 2010; Raulin et al., 2010b; Lay and Shao, 2011; Vadas et al., 2012], while others are periodic, created by natural oscillations like the 11-year solar cycle and the annual cycle [e.g., Hauchecorne et al., 1991; Thomson and Clilverd, 2000].

The annual cycle in the mesopause temperatures has been studied and is well understood, with the local mesopause temperatures reaching a minimum in summer, and maximum in winter [Kelley, 2009]. Tides and gravity waves propagating into the mesopause from lower atmospheric layers are the major source of turbulence in this region [Lindzen, 1981]. The atmospheric wind profile in the winter hemisphere allows predominantly westward propagating gravity waves to travel vertically and break into the mesopause, thus depositing westward momentum into the region. This momentum deposition together with the Coriolis effect create a circulation between the two hemispheres that demands a downward flow in the winter hemisphere, resulting in adiabatic warming of the mesopause in that hemisphere [Kelley, 2009]. The opposite effect occurs in the summer hemisphere, resulting in the adiabatic cooling of the mesopause in summer. The combination of the above circulation, along with the weak solar heating that causes the low temperatures of the region, and the ineffective (due to the low temperatures) infrared cooling response to the temperature gradient, which is created by the circulation, all cause the cold mesopause to have extremely strong temperatures differences between the two poles [Smith, 2004].

In addition to the mesopause temperatures, the electrical conductivity of the mesopause region also exhibits an annual cycle. The main sources for ionization of the ionospheric D and E layers are solar Extreme Ultra Violet (EUV) and X-ray radiation [Hargreaves, 1995]. However, the ionosphere's composition is also affected by the medium's temperature and density [Taubenheim, 1983; Hargreaves, 1995; Kopp, 2000; Kamide and Chian, 2007]. Since the available incoming solar radiation is a function of the solar zenith angle, which depends on the latitude, time of day, and stage of the annual cycle [Kopp, 2000], the ion composition and therefore also the electrical conductivity of the region depend on the time of year.

The high concentrations of electrons and ions in the ionosphere makes it act as a conductor, particularly for lower frequency electromagnetic waves [Appleton, 1932; Reuveni and Price, 2009]. As a result, the layer of air between it and the conductive Earth acts as an electromagnetic waveguide for very low frequency (VLF) waves [Hargreaves, 1995; Williams and Satori, 2007]. Therefore, modifications of the conductivity in the D-layer will influence VLF signals propagation [Ahrens, 2000; Inan et al., 2010].

VLF signals in the atmosphere are generated both by man-made sources (e.g. VLF communication transmitters) and by natural sources (e.g. lightning discharges) [Barr et al., 2000]. They can travel within the Earth-ionosphere waveguide over long distances (tens of megameters) with low attenuation (~2 dB per Mm), being reflected between the D-layer of the ionosphere and the Earth's surface [Wait, 1957b; Rodger and McCormick, 2006]. Because VLF received signals inherently contain information of the reflection height's region and its variability [Inan et el., 2010], their measurements allow monitoring the D-layer near the mesopause, and its variability.

This paper looks at the connection between mesopause temperatures and the amplitude of VLF narrowband (NB) signals.

2. Instrumentation

2.1 VLF antennas

The primary VLF receiver stations used in this study are located in two different sites in Israel. The first is located at the Emilio Segre' Observatory of the Israeli Cosmic Ray and Space Weather Center, at Mt. Hermon (MH) in the north part of Israel (33.18ºN, 35.47ºE), and is part of the AWESOME network described in Cohen et al. [2010]. Its antenna is built from two orthogonal triangular loop antennas. Each loop has a baseline of 2.6 meters, and 1.3 meters height, giving an area of approximately 1.69 m^2 for each loop, and has a total number of 12 turns. The loop antenna impedance is 0.85 mH and 1 Ω.

The second receiver is located at the Desert Research Institute of Ben-Gurion University, at Sde-Boker (SB) in the Israeli Negev Desert (30.5ºN, 34.4ºE). It has International Geophysical Year type loop antennas, and is similar to the antenna at Palmer Station, Antarctica, operated by Stanford University's VLF group [Reising et al., 1996]. Each of the two orthogonal loops has a baseline of 18 meters, and 9 meters height, giving an area of approximately 81 m^2 for each loop, which is single turned. The loop antenna impedance is 65 mH and 0.061 Ω.

In addition to the primary VLF stations mentioned above, data from additional VLF receivers were used in this study. One is located in Crete (CR), Greece (35.3ºN, 25.1ºE) and is also part of the Stanford University VLF AWESOME network. Another is located in Dunedin (DN), New Zealand

(45.8ºS, 170.5ºE), is part of the AARDDVARK network [Clilverd et al., 2009] and is operated by the University of Otago.

In all antennas, one loop is aligned in the north-south direction of propagation, and the other in the east-west direction of propagation. The data acquisition of signals received by each antenna is made using software that records NB data at specific frequencies (frequencies which correspond to VLF communication transmitters around the world). The NB data used and analyzed in this study were generally continuously recorded at a rate of 1 Hz.

2.2 The SABER instrument

The SABER (Sounding of the Atmosphere using Broadband Emission Radiometry) instrument which is on-board the TIMED (Thermosphere-Ionosphere-Mesosphere Energetics and Dynamics) satellite, was launched in December 2001 and has collected data more or less continuously since January 2002 [Riggin et al., 2006]. SABER is a 10 channel broadband, limb-viewing, infrared radiometer [Mlynczak, 1997]. It views the atmosphere at a right angle to the satellite velocity vector, so that as a result of the satellite's nearly circular orbit at an altitude of 625 km and with an inclination of ~74º, the latitude coverage of the instrument on a given day extends from about 53º latitude in one hemisphere to 83º in the other [Russel III et al., 1999; Siskind et al, 2005; Zhang et al., 2006]. This viewing geometry alternates every 60 to 63 days due to 180º yaw maneuvers required for the TIMED satellite [Zhang et al., 2006; Remsberg et al., 2008]. Thus, SABER generally provides continuous measurements for the latitudes of ±53º.

Among other parameters, such as ozone, water vapor, carbon dioxide, nitric oxide, and airglow emissions, the SABER instrument provides measurements of the temperature at altitudes from ~16-~120 km (with an accuracy of ~1-2 K), using the CO_2 15 μm wavelength emission [Mlynczak, 1997; Russel III et al., 1999; Garcia et al., 2005; Siskind et al., 2005; Riggin et al., 2006; Zhang et al., 2006]. These temperature profiles were used in the current study for comparison with the VLF NB data.

3. Methodology

As mentioned above, variations in the received VLF NB signals depend on the Earth-ionosphere waveguide conditions i.e., mainly the electron number density profile in the ionosphere's D-layer. Changes in the electron number density (henceforth electron density) profile itself or its altitude cause the VLF reflection height to change, as VLF waves tend to reflect at an electron number density of roughly 300 electrons cm^3 [Mambo et al., 1983]. VLF communications transmitters, that broadcast continuous signals from a fixed location with a constant amplitude and frequency, enable the monitoring of the ionosphere's D layer, and hence the mesopause region along the Great Circle Path (GCP) between the transmitter and the VLF antenna. In addition, changes in the electron density profile within the D-layer cause the phase of the received transmitter's wave to change [e.g., Raulin et al., 2010a; Raulin et al., 2010b]. According to Rishbeth [1990] and Lastovicka et al. [2006], a future thermal cooling of the thermosphere due to stronger radiative cooling by higher concentrations of greenhouse gases, will result in the decrease of ionospheric layer heights. This possible climate change effect on VLF amplitudes was the key motivation for the comparison between the SABER temperature data and the received VLF transmitter signal amplitude.

For this study, we limit ourselves to considering a small number of VLF transmitters. Each transmitter is know by a three-letter callsign, which for the case of transmitters considered here are: NWC (North West Cape, Australia, 19.8 kHz), NRK (Grindavik, Iceland, 37.5 kHz), NSC (Sicily, Italy, 45.9 kHz), and DHO (Rhauderfehn, Germany, 23.4 kHz). NB VLF amplitude data corresponding to several paths (different transmitters and receivers) were used and analyzed. The data sets were chosen so that during each period, the VLF data were fairly complete, and the transmitter was operating at the same power. To be consistent, one hour averages of daytime VLF amplitude were used (12-13 UT for all paths except DN-NWC, for which 23-00 UT was taken), in order to represent the sunlit "daily" amplitude value. This period was chosen for being close to local midday, the most stable VLF amplitude period of the day, when solar radiation dominates the ionization processes in the ionospheric layers [Kamide and Chian, 2007]. This stable period is seen in Figure 1, which shows the signal received at MH on 7 October 2011 from the NSC transmitter, located in Sicily, Italy. It is clearly seen that the one-hour averaged window (marked by the red rectangle and arrow) is representative of a stable reception period during the day.

(Figure 1)

In order to gather sufficient SABER data that will best represent the atmosphere along the GCP, each GCP was arbitrarily split into 11 boxes, where the transmitter and receiver lie at the center of the edge boxes, with approximate width of 10 degrees longitude as illustrated in Figure 2 for the SB-DHO and MH-NSC paths. The SABER data used consists of all the temperature data (day and night) within the boxes, in the altitude range of 17-100 km. Although the VLF data was taken only for one specific hour during the day, all of the SABER data was used. That is because observations made by the SABER instrument, as with any polar-orbiting satellite, provide snapshots of data, with measurements at different locations made at different universal times [Garcia et. al., 2005]. Moreover, the measurement time at a specific location is not constant each day and tends to vary. Finally, because of the relatively small size of the boxes, the number of SABER data samples along the GCP for each day are relatively low, and do not always consist of data from all of the boxes. Therefore, in order to use a reliable measure that will best represent the average temperature along the GCP, the entire SABER data along the path was used. The above limitation of the SABER data will be further discussed in the Discussion section. Figure 3 shows an example of the SABER temperature data for the MH-NSC data set. The atmospheric regions up to the mesopause can be clearly seen, as well as the cooling and warming of the mesopause during the hemispheric summer and winter, respectively. Note the variability in the stratosphere and stratopause temperatures in winter months, while calm conditions prevail in the summer months.

(Figure 2)

(Figure 3)

Each data set corresponding to a certain transmitter-receiver path was smoothed by a 15-20 day running average (in consideration of the data set length and the available amount of VLF data). The SABER data was divided into vertical layers, each one 3 km thick. We then compared the temperature and the daily average NB VLF amplitude time series, searching for the SABER altitudes which showed the highest correlations with the VLF data (negative and positive). It should be noted that the (Pearson's) R correlation coefficient was calculated for independent points, i.e., each point represent 15-20 measurement days, which were averaged only for this point. Thus, the correlation represents mainly the parameters seasonal behavior.

4. Results

4.1 Temperature-VLF correlations

The VLF amplitude data and the SABER temperature profile were analyzed and compared for each SABER layer and transmitter-receiver GCP. Figure 4 shows the 20-day-running-average of VLF amplitude (black curve), together with the time series of the SABER layers with maximum correlation (negative and positive) for three data sets (SB-DHO 2009, DN-NWC 2006-2007, and MH-NSC 2009-2011). All parameters were normalized (values between zero to one) to better visualize the similarity in the data sets behavior (the VLF amplitudes were normalized from their dB values). The gaps in the plots are due to gaps in the VLF data and so the temperature values weren't plotted during these gaps in order to give a true perspective of the available data for comparison. The seasonal cycle can be clearly seen in all of the time series as the most dominant pattern. In the data sets which are illustrated in Figure 4, a very high correlation was found between the VLF amplitude data and SABER measured temperatures for altitudes around 30-40 km. In addition, a very high negative correlation was found between VLF data and mesopause temperatures around 80-90 km altitude. Thus, a decrease/increase in the VLF amplitude usually comes hand-in-hand with a decrease/increase of the temperatures in the stratosphere layer, and with an increase/decrease of the temperatures at the mesopause layer. This behavior can be seen not only in the annual scale, but many times also in shorter time scales, as demonstrated in Figure 4. Note the remarkable mirror-like similarity between the behavior of the VLF amplitude and mesopause temperatures in the DN-NWC 2006-7 data set (Figure 4b).

(Figure 4)

The maximum positive correlations between the temperatures and amplitudes were found for altitudes mostly in the stratosphere and lower mesosphere, even though VLF waves are not reflected off these atmospheric layers. In contrast, the statistically significant maximum negative correlations were mostly located around the mesopause, above the typical daytime VLF reflection altitude. These results are summarized in Table 1, showing the time series dates, the number of running average days, the value of the Pearson's R correlation coefficient, the corresponding altitude for the maximum negative correlation, and the statistical significance ($p_{val}<0.05$). As seen in Figure 4, the dominant effect on both the temperature and the VLF amplitude is the annual cycle. The four data sets that showed correlation with layers other than the mesopause (see Table 1), usually had VLF amplitude behavior that did not follow the typical annual pattern. Nevertheless, for these data sets there were also time periods which showed the negative correlation between VLF amplitude and mesopause temperatures seen on the other transmitter-receiver paths. It should be mentioned that the highly variable local midnight VLF data was also compared to the SABER temperature data, and gave very similar results, though noisier. Hence, the authors decided not to include that analysis in this paper.

Date set	**Data set period**	**Days of running average**	**Max negative R correlation coefficient**	**Max Negative correlation Altitude [km]**	**Significant ($P_{val}<0.05$)**
SB-NRK2007	**23/03/2007-31/08/2007**	15	-0.664	23-26	x
SB-NRK2008	**08/04/2008-02/08/2008**	15	-0.977	74-77	√
SB-NRK2009	**10/05/2009-10/12/2009**	20	-0.828	89-92	√
SB-DHO2007	**23/03/2007-31/08/2007**	15	-0.810	65-68	√
SB-DHO2008	**08/04/2008-02/08/2008**	15	-0.938	77-80	√
SB-DHO2009	**10/05/2009-10/12/2009**	20	-0.890	86-89	√
SB-DHO2010	**12/04/2010-02/08/2010**	15	-0.926	26-29	√
SB-NSC2007	**23/03/2007-31/08/2007**	15	-0.834	80-83	√
SB-NSC2008	**08/04/2008-02/08/2008**	15	-0.999	44-47	√
SB-NSC2009	**10/05/2009-10/12/2009**	20	-0.914	86-89	√
SB-NSC2010	**12/04/2010-02/08/2010**	15	-0.758	35-38	x
SB-NWC2009	**10/05/2009-10/12/2009**	20	-0.567	77-80	x

MH-NSC2009-2011	**01/04/2009-31/04/2011**	20	-0.509	86-89	√
DN-NWC2006-2007	**0106/2006-31/05/2007**	20	-0.888	80-83	√
CR-DHO2008-2009	**01/08/2009-31/12/2009**	20	-0.846	95-98	√

Table 1: VLF and SABER temperature data sets negative correlation summary.

4.2 Principle Component Analysis (PCA) of mesopause temperature, VLF amplitude, and solar irradiance

As mentioned in the introduction, solar irradiance has a large impact on the UMLT region. It effects both the mesopause temperatures and the D-region's composition by its entire spectrum, e.g., ionization of NO molecules at the D-region by radiation at a wavelength of 121.5nm (the Lyman-α emission line) [Kamide and Chian, 2007], chemical heating of the mesopause by photolysis of ozone as a result of incoming radiation at wavelengths shorter than 238nm [Smith, 2004], etc. It is also well known that VLF propagation can be described through solar zenith angle-dependent variations in D-region electron density [e.g., Thomson, 1993].

Because of the many processes and reactions in the atmosphere and ionosphere (also above the UMLT region) as a result of solar irradiance, we decided to take into account the incoming solar radiation, i.e., total solar irradiance (TSI), as function of the solar zenith angle, as described in the equation:

$$I_{in} = I_{TOA} e^{-\sec\chi} \tag{1}$$

Where I_{in} is the incoming solar radiation, I_{TOA} is the total solar irradiance (TSI) at the top of the atmosphere (TOA), and χ is the solar zenith angle.

TSI data measured by NASA's SORCE (SOlar Radiation and Climate Experiment) satellite and calculated for Earth's TOA was used for I_{TOA}, and the zenith angle was calculated based on the time of year, for the midpoint of the GCP at 12:30 UT (23:30 UT for Dunedin), in order to be consistent with the mean hour of day of the VLF amplitude.

In order to examine the mutual dependencies of the three parameters, i.e., solar insolation, VLF amplitude, and mesopause temperatures (represented in this section by SABER 80-90 km mean temperature data along the GCP, where most of the anti-correlations existed in the former section, even though it is above the daytime VLF reflection height [McRae and Thomson, 2000]), Principle Component Analysis (PCA) was performed on each data set. Before initiating the PCA, the SABER temperature and VLF amplitude data gaps, which were caused by power failures, VLF transmitters that stopped broadcasting as part of their regular maintenance cycle, lack of satellite overpasses, etc., were filled with the use of harmonic analysis [Wilks, 2006]. The few gaps in the SORCE data were filled with the Cubic Spline interpolation. All the parameter's time series were standardized, i.e., scaled so that each data set variance was made equal to one, to make the PCA not emphasize the parameter with the largest variance. It should be noted that there was no additional smoothing undertaken (e.g., running average, etc), beyond the processing described earlier.

The PCA results for the SB-DHO 2009, DN-NWC 2006-7, and MH-NSC 2009-11 data sets are demonstrated in Figure 5, showing the time series of each Principle Component (PC) multiplied by the PC coefficient of each parameter, thus visualizing the amount of representation (or strength) of that parameter in that PC. Each PC explains a certain amount of the variance of the whole data set. This amount was calculated by the ratio of the examined PC root to the sum of all PCA roots. Thus for example, for the data sets shown in Figure 5, PC_1 which obviously shows the pattern of the annual cycle, explains ~77% of the variance of SB-DHO 2009 data set, ~75% of the variance of DN-NWC 2006-7, and ~60% of the variance of MH-NSC 2009-11 data set. It can be seen that the VLF is in phase with the solar insolation and opposite to the mesopause temperatures, similar to what was seen in Figure 4 as the dominant behavior. PC_2 shows for the three illustrated data sets a very weak participation of the solar insolation, thus hinting that the origin of these variations seen in the VLF amplitudes and mesopause temperatures, is not connected to the solar cycle. PC_3 shows strong involvement of the temperature and the solar irradiance, opposite to the relatively weak VLF participation, possibly indicating a positive feedback between the solar insolation changes and mesopause temperature, effecting ~10% of its variance.

(Figure 5)

The PCA, done on all of the data sets gave similar results. Most of the PCs showed the same patterns as those seen in Figure 5, and described in the paragraph above. The explained variance of the PCs was also around the same values. Table 2 summarizes the explained variance of the PCs of each data set. It also shows indices used in Figure 6, which illustrates graphically the explained variance of each of the 15 data sets PCs. It can be seen that while SB-DHO 2009 had the highest explained variance from PC_1 and SB-NSC 2008 has the lowest value, the explained variance of PC_1 is around ~60%, the average value of that PC. As described, this PC is well attributed to the solar annual cycle and hence, this average value hints about the indirect global solar influence on the VLF and mesopause temperatures (through gravity waves and tidal forcing, as described in the Introduction section). Because of the strong involvement of the solar insolation in PC_3, it can be deduced that an additional ~11% (on average) of the data variance (mostly in the mesopause temperature) are affected by the solar insolation changes with a positive feedback, contrary to the negative feedback in PC_1. Finally, because it usually exhibits almost no participation of the solar insolation, PC_2's average value of ~28% indicates that this is the amount of other short time scale forcings on the daytime VLF amplitude and mesopause temperature, which are not connected to the TSI (see Discussion section).

Table 2: PCA explained variance summary and data set indices for figure 6. See text for details.

Figure 6 index	Data set	PC1	PC2	PC3
1	**SB-DHO2007**	60.92%	30.95%	8.13%
2	**SB-DHO2008**	59.80%	26.94%	13.26%
3	**SB-DHO2009**	77.19%	15.20%	7.60%
4	**SB-DHO2010**	53.02%	31.73%	15.25%
5	**SB-NRK2007**	65.63%	29.89%	4.48%
6	**SB-NRK2008**	62.27%	29.83%	7.90%
7	**SB-NRK2009**	67.62%	25.70%	6.68%
8	**SB-NSC2007**	55.09%	28.49%	16.42%
9	**SB-NSC2008**	44.12%	33.66%	22.23%
10	**SB-NSC2009**	53.45%	32.15%	14.40%
11	**SB-NSC2010**	53.27%	33.28%	13.45%
12	**SB-NWC2009**	58.24%	27.92%	13.83%
13	**MH-NSC2009-11**	59.62%	28.44%	11.94%
14	**DN-NWC2006-7**	74.58%	17.95%	7.47%
15	**CR-DHO2008-9**	60.18%	33.58%	6.24%
Average:		**60.33%**	**28.38%**	**11.28%**

(Figure 6)

5. Mesopause temperature estimation using the PCA

As concluded from this analysis, ~72% of the mesopause temperature variability is attributed to global long term solar influence, while the residual ~28% are attributed to other short term forcings that also affect the measured VLF NB amplitudes. Using these results, we attempted to estimate the mesopause temperatures using only the VLF and TSI data.

For the temperature estimation to be made, a PCA (without prior execution of harmonic analysis on the data) has been performed on the first 80% of each data set. The residual 20% at the end of the data set were then used to estimate the mesopause temperatures, and compared to the available SABER data, corresponding to the same dates.

Generally speaking, the temperature estimation model used the sum of two linear polynomial fits y_1+y_2, where the y_1 and y_2 polynomials may be described by the equations

$$\left(Coeff_{T_{PC_2}} \cdot Score_{T_{PC_2}}\right) \cdot S_{T_1} = y_1 = a\left(Coeff_{VLF_{PC_2}} \cdot Score_{VLF_{PC_2}}\right) \cdot S_{VLF} + b \quad (2)$$

$$\begin{gathered}\left(Coeff_{T_{PC_1}} \cdot Score_{T_{PC_1}} + Coeff_{T_{PC_3}} \cdot Score_{T_{PC_3}}\right) \cdot S_{T_2} = y_2 = \\ c\left(Coeff_{I_{PC_1}} \cdot Score_{I_{PC_1}} + Coeff_{I_{PC_3}} \cdot Score_{I_{PC_3}}\right) \cdot S_I + d\end{gathered} \quad (3)$$

Where '*T*' is an index for temperature, *'VLF'* stands for the VLF amplitude, and '*I*' stands for the solar insolation. '*a*', '*b*', '*c*' and '*d*' are the polynomial's coefficients, *'Coeff'* and *'Score'* are the PC coefficients and the PC time series for the parameter and its PC number in the subscript. '*S*' represents a scaling procedure done in consideration of the explained variance of the PC used for the linear fit (PC_2 for y_1 and PC_1+ PC_3 for y_2), and the known mesopause temperature data. The error was taken as the standard deviation of the estimated temperatures.

The execution of the temperature estimation procedure showed that in 6 out the 15 data sets, the procedure resulted in statistically significant agreement with the known values of the mesopause temperatures. However, even when the absolute values did not agree, the estimated temperature variability appeared to often follow the true temperature behavior. Figure 7 shows the time series plot of the estimated temperatures of the SB-DHO 2010 data set. SB-DHO 2010 was the data set which gave the best results with a significant R=0.7 correlation coefficient. The PCA for that data set was made over the first 67 data points out of the 84 of the whole data set, while the last 17 were estimated (Figure 7). The SABER temperature error bars were calculated for each point as the standard deviation of the temperature values, which were averaged for that point's temperature value. The estimated temperatures seem to follow rather well the SABER true values, with a 3.9 K mean difference between the true and estimated values.

(Figure 7)

6. Discussion

This study was made using data gathered by the SABER instrument and ground-based VLF antennas, in order to find a link between atmospheric temperatures and VLF NB amplitudes. The first comparison between VLF NB amplitude and the SABER temperature profile showed that in most cases the highest anti-correlation was between the NB amplitudes and mesopause temperatures. Although VLF NB amplitudes were already associated in previous studies to the dynamics and temperatures of the stratosphere [e.g., Correia et al., 2011], the relation between VLF NB amplitudes and mesopause temperatures, either direct or indirect, has not been identified previously. However, a connection between mesopause temperatures and radio waves absorption has been predicted before [e.g., Taubenheim, 1983].

The results were presented here for long term time scales, showing clearly the effect of the solar annual cycle. Additional analysis of the data (not presented here) was made, where the annual cycle effects were removed by subtracting the 30-days running average of the data from the unsmoothed data. This analysis showed that after the removal of the annual cycle, there were still several periods, up to nine weeks, where the VLF amplitude and the mesopause temperature changes anti-correlated extremely well, in a way similar as shown in Figure 4. While the reason for this relation between the two parameters is quite elusive, modal interference and signal absorption may account, at least to some extent, for these intriguing results.

Modal interference has an important effect on the received amplitude of VLF signals, as the received amplitude is the sum of several waveguide modes [Wait, 1957a]. The signal might be strongly attenuated if destructive modal interference occurs, which depends on the waveguide's characteristics and the distance between the transmitter and receiver. A change in the VLF reflection height which might happen together with a vertical displacement of atmospheric layers, i.e., a downward/upward displacement of the reflection height occurring together with adiabatic warming/cooling of the region, will change the modal interference pattern and therefore, the amplitude of the received signal. This effect can be examined by running the Naval Ocean Systems Center (NOSC) LWPC (Long Wave Propagation Capability) model [Ferguson, 1998]. We ran the LWPC for each GCP that was analyzed in this study, in order to examine the amplitude change if the reflection height is displaced up or down from its "default" value. We decided to represent the default ionosphere in the model with the parameter values of β=0.3 km^{-1} (exponential sharpness factor) and h'=74 km (linked to the reflection height), which according to McRae and Thomson [2000] are typical daytime values for low-mid latitudes during solar minimum (all analyzed data sets were around the last solar minimum). The results of the LWPC model runs are illustrated in Figure 8. It can be seen that for five out of six GCPs, there is a positive dependence between h' and the VLF amplitude around the default values, i.e., an upward/downward displacement of the reflection height results in a higher/lower received signal amplitude, thus matching the data sets analysis. Nevertheless, this rise of the received signal is rather weak, not exceeding ~0.5 dB/km (except SB-NRK, where the rise is ~2 dB/km). However, CR-DHO GCP seemed to show an opposite behavior, although the data set of this GCP showed a similar anti-correlation pattern with temperature like most other data sets. Therefore, we conclude that modal interference cannot be the main and only reason for the good correlation between mesopause temperatures and VLF amplitudes. However, it may explain the data sets where the mesopause temperatures had a positive correlation with the VLF amplitudes or very weak anti-correlation, if the "default" h' was shifted by a few kilometers up or down.

(Figure 8)

On the other hand, VLF absorption might also play a role in the observed day-to-day anti-correlation between UMLT temperatures and VLF NB amplitudes. The absorption coefficient κ refers to the distance over which the amplitude of a radio signal drops by a factor of 1/*e* from its original magnitude. For VLF waves $\kappa \propto N_e/\nu$ where N_e is the electron density and υ is the electron-neutral collision frequency [Hargreaves, 1995]. According to McCormick et al. [2002] $\nu \propto [X] \cdot T_e^{n(X)}$ where [*X*] is the abundance of an atmospheric neutral species *X*, T_e is the electron temperature, and *n(X)* is a positive number that depends on the species. In the model used by Rodger et al. [1998] and Rodger et al. [2007] the change in the electron density N_e is described by the equation

$$\frac{\partial N_e}{\partial t} = q - \beta N_e - \alpha N_e^2 \tag{4}$$

Where q is the ionization rate, α is the recombination coefficient, and β is the attachment rate. As for their dependencies with temperature, $\alpha \propto 1/T_e^m$ where m is a positive number which depends on altitude, and β is a function of T_e, T_n (neutral's temperature), and the atmospheric species chemical reaction [Rodger et al., 1998; Rodger et al., 2007]. Thus, α decreases as T_e increase, and β might decrease as T_e increase, thus resulting in a higher electron density.

Since electrons thermalize very quickly in the D region, we take $T_e = T_n$. By examining the absorption coefficient dependencies over the temperature which were described in the last paragraph, we can see that as the temperature (in the D-region) increases, υ increases and so does the change in electron density $\partial N_e/\partial t$. In a situation where N_e is more sensitive to the temperature than υ, a higher temperature will result in a higher κ and hence, a lower received VLF amplitude, matching the results of this study. Certainly, this is a rather simplified approach which can only arrive at qualitative conclusions.

To summarize, both mechanisms together, i.e., modal interference and signal absorption, are potentially capable in explaining, at least qualitatively, the connection between VLF received amplitudes and mesopause temperatures. They may also explain the opposite connection seen in some data sets, where the mesopause temperatures had a positive correlation with the VLF amplitudes, by a change in the typical reflection height or by the collision frequency governing the electron density. However, the dependencies seen in both mechanisms are not linear, as the correlation found from this study's analysis show, but rather exponential and more complex. Thus, it may be possible that other mechanisms are responsible together with those presented here, which may result in the connection between temperatures and VLF amplitudes. Obviously, this topic needs more study which, however, is beyond the scope of the present paper.

With respect to the UMLT temperature and VLF amplitude, both are known to vary, either directly or indirectly, as a function of solar irradiance. In order to examine the amount of solar influence on these quantities, PCA has been performed on the calculated solar insolation, the VLF amplitude and the mesopause (80-90 km SABER) temperatures. The PCs time series together with the explained variance have shed some light on the external forcing of the examined quantities, disassembling the acquired signals to their root patterns. It was concluded from this analysis that ~72% of VLF/mesopause temperature's fluctuations are affected by solar irradiance changes on large spatial and temporal scales, while 28% of the changes are a result from other short time scale forcings. These forcings may be external such as solar flares (that cannot be noticed in the TSI, as most of their energy is emitted in the EUV and X-ray wavelengths), or internal, e.g., particle precipitation, red sprites, gravity waves, tides, etc. [Barr et al., 2000; Inan et al., 2010]. Because the VLF data was 1-hour-averaged, the very short phenomena, i.e., red sprites, particle precipitation, etc. are less likely to affect the amplitude values used in this analysis. In addition, while solar flares do exist during solar minimum, it is less likely that solar flares had significant influence on the PCA, due to the weaker and less frequent flares at solar minimum. Therefore, we may infer that the residual 28% of the measured variations are most likely the result of mainly internal sources such as gravity waves and atmospheric tides.

Using the PCA results, a simple model for mesopause temperature estimation was developed. The estimated temperatures were often close to the SABER values and also followed the temperature behavior and day-to-day changes. Nevertheless, most of the data sets did not show a statistically significant correlation between the true and estimated temperature values, and sometimes even showed an opposite behavior. However, there seems to be some basis and need for additional work on the topic.

With all of the invested work for this study, there are several issues which were beyond the capabilities of the authors which eventually, might have caused some bias in the results. These include the low amount of daily overpasses of the TIMED satellite and hence, the low spatial and temporal resolution of the SABER data may have caused inaccuracies in the temperature along the various transmitter-receiver GCPs. Also, the daily amount of vertical temperature profile "snapshots" taken by SABER was rather poor, with an average of 2-4 per day, thus creating a situation where 2-4 data boxes (see Figure 2) represent the whole GCP, which was represented by 11 data boxes. This bias was avoided using the 15-20 days running average which represented better the whole GCP, but in the other parts of this study (PCA and temperature estimations), the opportunity to do the same was not possible. Additional problems with the SABER data, which were already mentioned in section 3, are that the snapshots at different locations are made at different universal times, and the measurement time at a specific location is not constant each day and tends to vary. Furthermore, comparing these data to the VLF and solar insolation data, which were taken for a specific time of day, may have introduced a bias in the analysis. The same analysis was tried using only the SABER measurements which were taken during day, thus dealing somehow with this bias, but the lack of data became too serious. Finally, the uneven representation of the GCP also resulted due to the polar orbiting nature of the TIMED satellite, which created a situation where large amounts of data for boxes around ~50º latitude were acquired, while data for boxes of latitudes higher than ~53º were rather poor.

Nevertheless, the results of this study, which are new, seem to be significant and important. Since the solar insolation value for the needs of the temperature estimation is a function of time and location (by using the average solar constant and equation (1)), VLF NB observations may provide a useful tool to estimate the values and variability of mesopause temperatures. This mesopause monitoring may be important in many aspects of UMLT studies, such as climate change. The observed cooling trend of the middle-mesosphere as a result of climate change is ten times stronger than the equivalent warming of the troposphere, thus resulting in a much higher signal-to-noise ratio in the mesosphere [Lastovicka et al., 2006]. Therefore, mesopause monitoring through VLF measurements might prove to be a good proxy for ongoing climate change. There are many VLF transmitters dispersed around the world, and many more receiving antenna [e.g., Clilverd et al., 2009; Raulin et al., 2009; Cohen et al., 2010], thus creating thousands of possible transmitter-receiver GCP. Thus, a high spatial and temporal coverage of mesopause temperatures, especially compared to polar satellite measurements, might be achieved at a comparatively low cost by further improving of the temperature estimation method, and by analyzing more and longer data sets. Each of these recommendations demand further studies and work to be done, which might be valuable for the atmospheric research community.

Acknowledgments: This research was partially supported by the Ministry of Science and Technology, Israel. The authors wish to thank the Stanford University VLF group for support in the construction of the VLF receiver stations at Sde-Boker, Mount.-Hermon, and Crete. We thank the Solar Energy Research Center of Ben Gurion University, Sde-Boker, Israel, for allowing us to use their facility for our VLF antenna and data collection.

7. References

Ahrens, C. D. (2000), *Essentials of Meteorology*, pp. 12, Brooks/Cole/Thomson Learning.

Appleton, E. V. (1932), Wireless studies of the ionosphere, *IEEE,* 7, 257-265, doi: 10.1049/pws.1932.0027.

Barr, R., D. L. Jones, and C. J. Rodger (2000), ELF and VLF radio waves, *Jr. Atmos. Sol. Terr. Phys.*, 62, 1689–1718.

Bittner, M., K. Hoppner, C. Pilger, and C. Schmidt (2010), Mesopause temperature perturbations caused by infrasonic waves as a potential indicator for the detection of tsunamis and other geo-hazards, *Nat. Hazards Earth Syst. Sci*., 10, 1431–1442.

Clilverd, M. A., C. J. Rodger, N. R. Thomson, J. B. Brundell, T. Ulich, J. Lichtenberger, N. Cobbett, A. B. Collier, F. W. Menk, A. Seppälä, P. T. Verronen, and E. Turunen (2009), Remote sensing space weather events: Antarctic-Arctic Radiation-belt (Dynamic) Deposition-VLF Atmospheric Research Konsortium network, *Space Weather, 7,* S04001, doi:10.1029/2008SW000412.

Cohen, M. B., U. S. Inan, and E. P. Paschal (2010), Broadband ELF/VLF Radio Reception With the AWESOME Instrument, *IEEE Trans. Geosci. Remote Sens.*, 48, no. 1, pp. 3-17, doi:10.1109/TGRS.2009.2028334.

Correia, E., P. Kaufmann, J. P. Raulin, F. Bertoni, and H. R. Gavilan (2011), Analysis of daytime ionosphere behavior between 2004 and 2008 in Antarctica, *Jr. Atmos. Sol. Terr. Phys*., 73, 2272-2278, doi:10.1016/j.jastp.2011.06.008.

Ferguson, J. A. (1998), Computer Programs for Assessment of Long-Wavelength Radio Communications, Version 2.0: User's Guide and Source Files, *Space and Naval Warfare System Center San Diego CA 92152-5001.*

Garcia, R. R., R. Lieberman, J.M. Russell III, and M.G. Mlynczak (2005), Large-scale waves in the mesosphere and lower thermosphere observed by SABER, *J. Atmos. Sci*., 62, 4384-4399.

Hargreaves, J. K. (1995), *The Solar-terrestrial Environment: An Introduction to Geospace – The Science of the Terrestrial Upper Atmosphere, Ionosphere, and Magnetosphere*, pp. 61-77, 98-111, 208-236, Cambridge Univ. Press.

Hauchecorne, A., M.-L. Chanine, and P. Keckhut (1991), Climatology and trends of the middle atmosphere temperature (33–87 km) as seen by Rayleigh lidar over the south of France, *J. Geophys. Res*., 96, 15297-15309, doi:10.1029/91JD01213.

Havnes, O., U. de Angelis, R. Bingham, C. K. Goertz, G. E. Morfill, and V. Tsytovich (1990), On the role of dust in the summer mesopause, *J. Atmos. Terr. Phys*., 52, 637-643, doi:10.1016/0021-9169(90)90058-U.

Inan, U. S., S. A. Cummer, and R. A. Marshall (2010), A survey of ELF and VLF research on lightning-ionosphere interactions and causative discharges, *J. Geophys. Res.*, 115, A00E36, doi:10.1029/2009JA014775.

Kamide, Y, and A. Chian (2007), *Handbook of the Solar-Terrestrial Environment*, pp. 189-214, 223, Springer-Verlag Berlin Heidelberg.

Kelley, M. C. (2009), *The Earth's Ionosphere: Plasma Physics and Electrodynamics*, pp. 346-350, Academic Press, Elsevier.

Kopp, E. (2000), A global model of positive and negative ions in the lower ionosphere, *Adv. Space Res.,* 25, 173-182.

Lastovicka, J., R. A. Akmaev, G. Beig, J. Bremer, and J.T. Emmert (2006), Global change in the upper atmosphere, *Science*, 314, 1253–1254.

Lay, E. H., and X.-M. Shao (2011), High temporal and spatial-resolution detection of D-layer fluctuations by using time-domain lightning waveforms, *J. Geophys. Res.*, 116, A01317, doi:10.1029/2010JA016018.

Lindzen, R. S. (1981), Turbulence and stress due to gravity wave and tidal breakdown, *J. Geophys. Res.,* 86, 9707-9714.

Mambo, M., I. Nagano, K. Nakamura, and T. Fukami (1983), A method of estimating the electron density profile of the D-layer from a knowledge of the VLF reflection coefficients, *Radio Sci.*, 18, 119-127, doi:10.1029/RS018i001p00119.

McCormick, R. J., C. J. Rodger, and N. R. Thomson (2002), Reconsidering the effectiveness of quasi-static thunderstorm electric fields for whistler duct formation, *J. Geophys. Res.,* 107, (A11), 1396, doi:10.1029/2001JA009219.

McRae, W. M., and N. R. Thomson (2000), VLF phase and amplitude: daytime ionospheric parameters, *Jr. Atmos. Sol. Terr. Phys*., 62, 609-618, doi: 10.1016/S1364-6826(00)00027-4.

Mlynczak, M. G. (1997), Energetics of the mesosphere and lower thermosphere and the SABER experiment, *Adv. Space Res*., 20, 1177-1183.

Ortland, D. A., P. B. Hays, W. R. Skinner, and J.-H. Yee (1998), Remote sensing of mesospheric temperature and $O_2(^1\Sigma)$ band volume emission rates with the high-resolution Doppler imager, *J. Geophys. Res.*, 103, 1821–1835.

Raulin, J. P., F. C. P. Bertoni, H. R. Gavilán, W. G. Day, R. Rodriguez, G. Fernandez, E. Correia, P. Kaufmann, A. Pacini, T. R. C. Stekel, W. L. C. Lima, N. J. Schuch, P. R. Fagundes, and R. Hadano (2010a), Solar flare detection sensitivity using the South America VLF Network (SAVNET), *J. Geophys. Res.*, 115, A07301, doi:10.1029/2009JA015154.

Raulin, J. P., F. C. P. Bertoni, H. R. Gavilán, and J. C. Samanes (2010b), Long-term and transient forcing of the low ionosphere monitored by SAVNET, *AIP Conf. Proc.*, 1286, 103-125, doi: 10.1063/1.3512872.

Raulin, J. P., P. Correia de Matos David, R. Hadano, A. C. V. Saraiva, E. Correia, and P. Kaufmann (2009), The South America VLF Network (SAVNET), *Earth, Moon, and Planets*, 104, 1-4, 247-261.

Reising, S. C**.**, U. S. Inan, T. F. Bell, and W. A. Lyons (1996), Evidence for continuing currents in sprite-producing cloud-to-ground lightning, *Geophys. Res. Lett*., 23, 3639-3642.

Remsberg, E. E., B. T. Marshall, M. Garcia-Comas, D. Krueger, G. S. Lingenfelser, J. Martin-Torres, M. G. Mlynczak, J. M. Russel III, A. K. Smith, Y. Zhao, C. Brown, L. L. Gordley, M. J. Lopez-Gonzalez, M. Lopez-Puertas, C.-Y. She, M. J. Taylor, and R. E. Thompson (2008), Assessment of the quality of the Version 1.07 temperature-versus-pressure profiles of the middle atmosphere from TIMED/SABER, *J. Geophys. Res.*, 113, D17101, doi:10.1029/2008JD010013.

Reuveni, Y., and C. Price (2009), A new approach for monitoring the 27-day solar rotation using VLF radio signals on the Earth's surface, *J. Geophys. Res*., 114, A10306, doi:10.1029/2009JA014364.

Riggin D. M., H. L. Liu, R. S. Lieberman, R. G. Roble, J. M. Russell III, C. J. Mertens, M. G. Mlynczak, D. Pancheva, S. J. Franke, Y. Murayama, A. H. Manson, C. E. Meek, R. A.

Vincent (2006), Observations of the 5-day wave in the mesosphere and lower thermosphere, *Jr. Atmos. Sol. Terr. Phys*., 68, 323-339, doi:10.1016/j.jastp.2005.05.010.

Rishbeth, H. (1990), A Greenhouse effect in the ionosphere?, *Planet. Space Sci.*, 38, 945-948.

Rodger, C. J., O. A. Molchanov, and N. R. Thomson (1998), Relaxation of transient ionization in the lower ionosphere, *J. Geophys. Res.*, *103*, 6969–6975, doi:10.1029/98JA00016.

Rodger, C. J., and R. J. McCormick (2006), Remote sensing of the upper atmosphere by VLF, *Sprites, Elves and Intense Lightning Discharges*, Nat. Sci. Ser., 225, pp. 167–190, Springer, Dordrecht, Netherlands.

Rodger, C. J., M. A. Clilverd, N. R. Thomson, R. J. Gamble, A. Seppälä, E. Turunen, N. P. Meredith, M. Parrot, J.-A. Sauvaud, and J.-J. Berthelier (2007), Radiation belt electron precipitation into the atmosphere: Recovery from a geomagnetic storm, *J. Geophys. Res.*,*112*, A11307, doi:10.1029/2007JA012383.

Russell III, J. M., M. G. Mlynczak, L. L. Gordley, J. Tansock, and R. Esplin (1999), Overview of the SABER experiment and preliminary calibration results, *Proc. SPIE Int. Soc. Opt. Eng*., 3756, 277– 288, doi: 10.1117/12.366382.

Siskind, D. E., L. Coy, and P. Espy (2005), Observations of stratospheric warmings and mesospheric coolings by the TIMED SABER instrument, *Geophys. Res. Lett.*, 32, L09804, doi:10.1029/2005GL022399.

Smith, A. K. (2004), Physics and chemistry of the mesopause region, *J. Atmos. Terr. Phys.*, 66, 839-857, doi:10.1016/j.jastp.2004.01.032.

Taubenheim, J. (1983), Meteorological control of the D region, *Space. Sci. Rev.*, 34, 397-411, doi: 10.1007/BF00168831.

Thomson, N. R. (1993), Experimental daytime VLF ionospheric parameters, *J. Atmos. Terr. Phys.*, 55, 173-184.

Thomson, N. R., and M. A. Clilverd (2000), Solar cycle changes in daytime VLF subionospheric attenuation, *Jr. Atmos. Sol. Terr. Phys*., 62, 601-608, doi:10.1016/0021-9169(93)90122-F.

Vadas, S., J. Yue, and T. Nakamura (2012), Mesospheric concentric gravity waves generated by multiple convective storms over the North American Great Plain, *J. Geophys. Res.*, 117, D07113, doi:10.1029/2011JD017025.

Wait, J. R. (1957a), The Mode Theory of VLF Ionospheric Propagation for Finite Ground Conductivity, *Proc. IRE* , 45, 760-767, doi: 10.1109/JRPROC.1957.278469

Wait, J. R. (1957b), The attenuation vs. frequency characteristics of VLF radio waves, *Proc. IRE*, 45, 768-771, doi: 10.1109/JRPROC.1957.278470.

Wilks, D. S. (2006), *Statistical Methods in the Atmospheric Sciences 2nd edition*, pp. 371-381, Academic Press, Elsevier.

Williams, E. R., and G. Sátori (2007), Solar rotation-induced changes in ionospheric height and the Schumann resonance waveguide on different timescales, *Radio Sci.*, 42, RS2S11, doi:10.1029/2006RS003494.

Yu, J. R., and C. Y. She (1995), Climatology of a midlatitude mesopause region observed by a lidar at Fort Collins, Colorado (40.6°N, 105°W), *J. Geophys. Res.*, *100*, 7441–7452, doi:10.1029/94JD03109.

Zhang, X., J. M. Forbes, M. E. Hagan, J. M. Russell III, S. E. Palo, C. J. Mertens, and M. G. Mlynczak (2006), Monthly tidal temperatures 20–120 km from TIMED/SABER, *J. Geophys. Res*., 111, A10S08, doi:10.1029/2005JA011504.

List of Figures:

β=0.3 km^{-1} and h'=74 km, for the GCPs which were examined in this study.

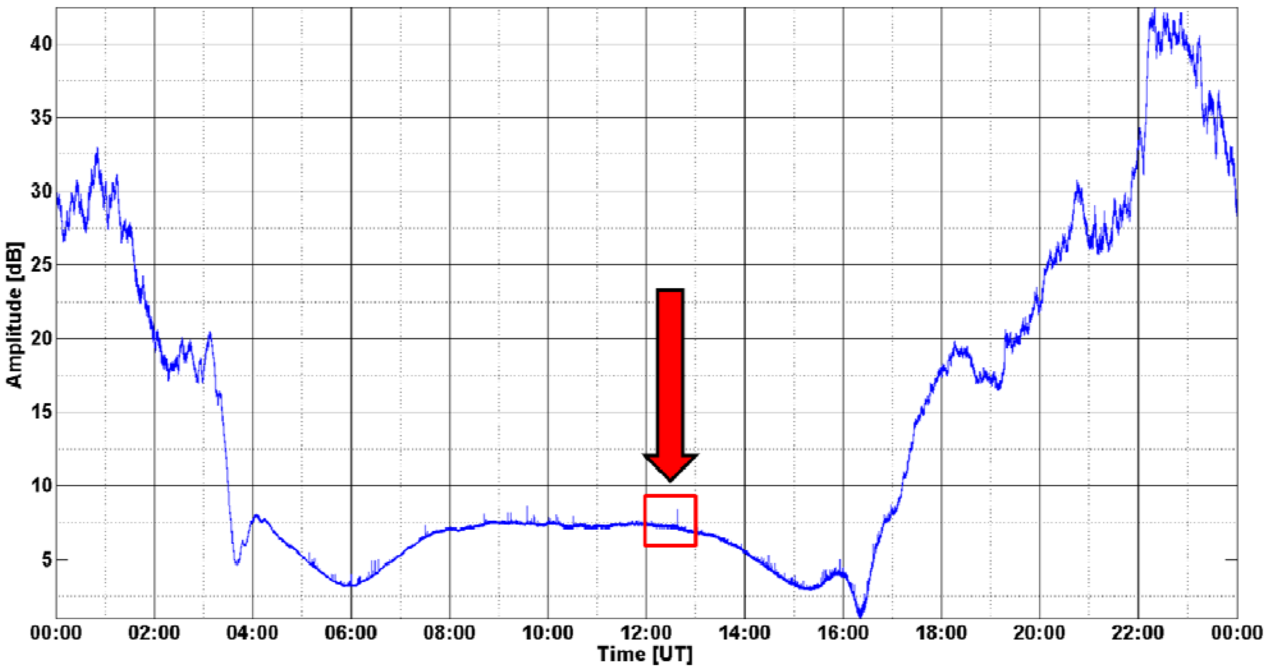

Figure 1: daily variation of the NSC transmitter (45.9 kHz) signal received at MH on 7 October 2011. The averaged one-hour window is marked by the red rectangle and arrow.

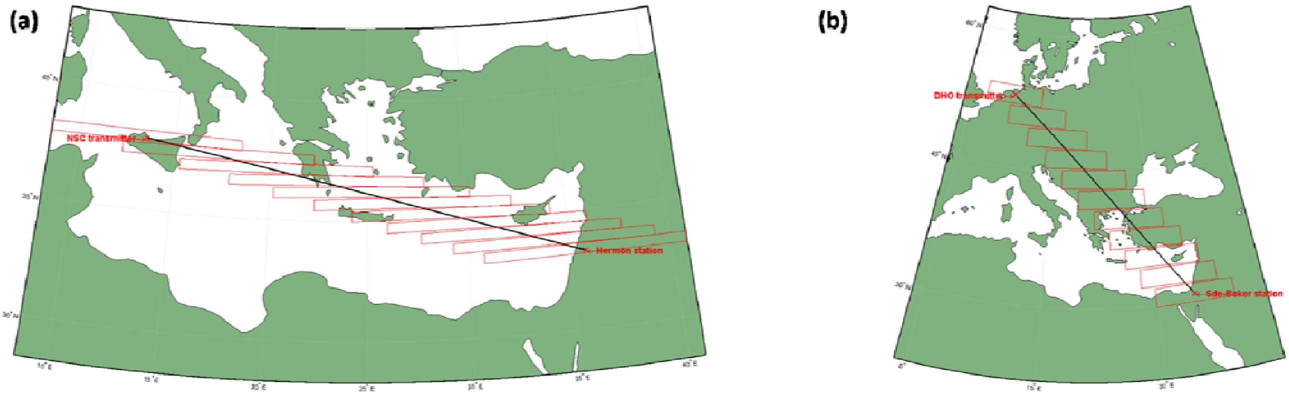

Figure 2: Transmitter-receiver GCP division into 11 SABER temperature data boxes for (a) MH-NSC and (b) SB-DHO paths.

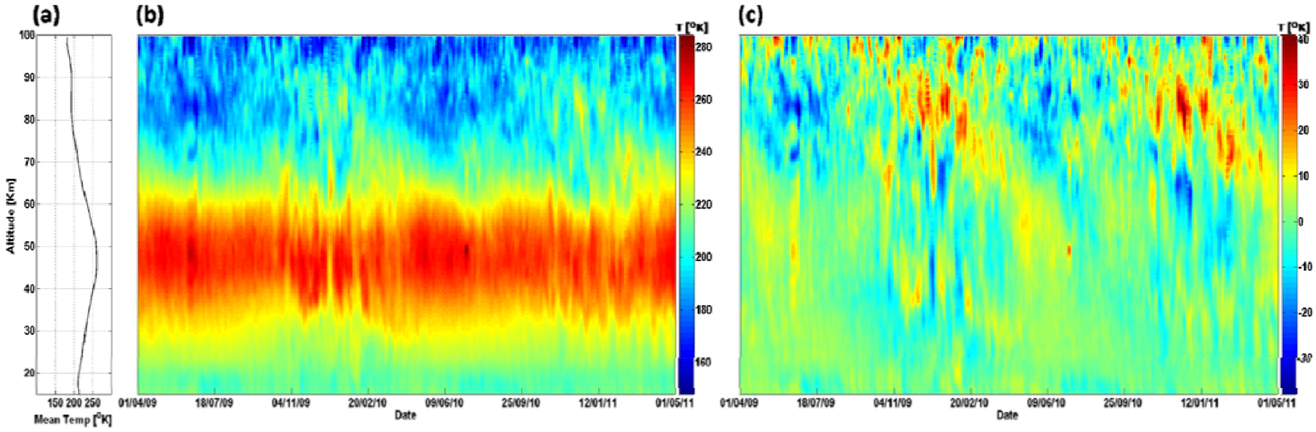

Figure 3: Saber data for MH-NSC path corresponding to the period of April 2009-April 2011 (a) average temperature profile (b) profile time series (c) profile anomalies time series.

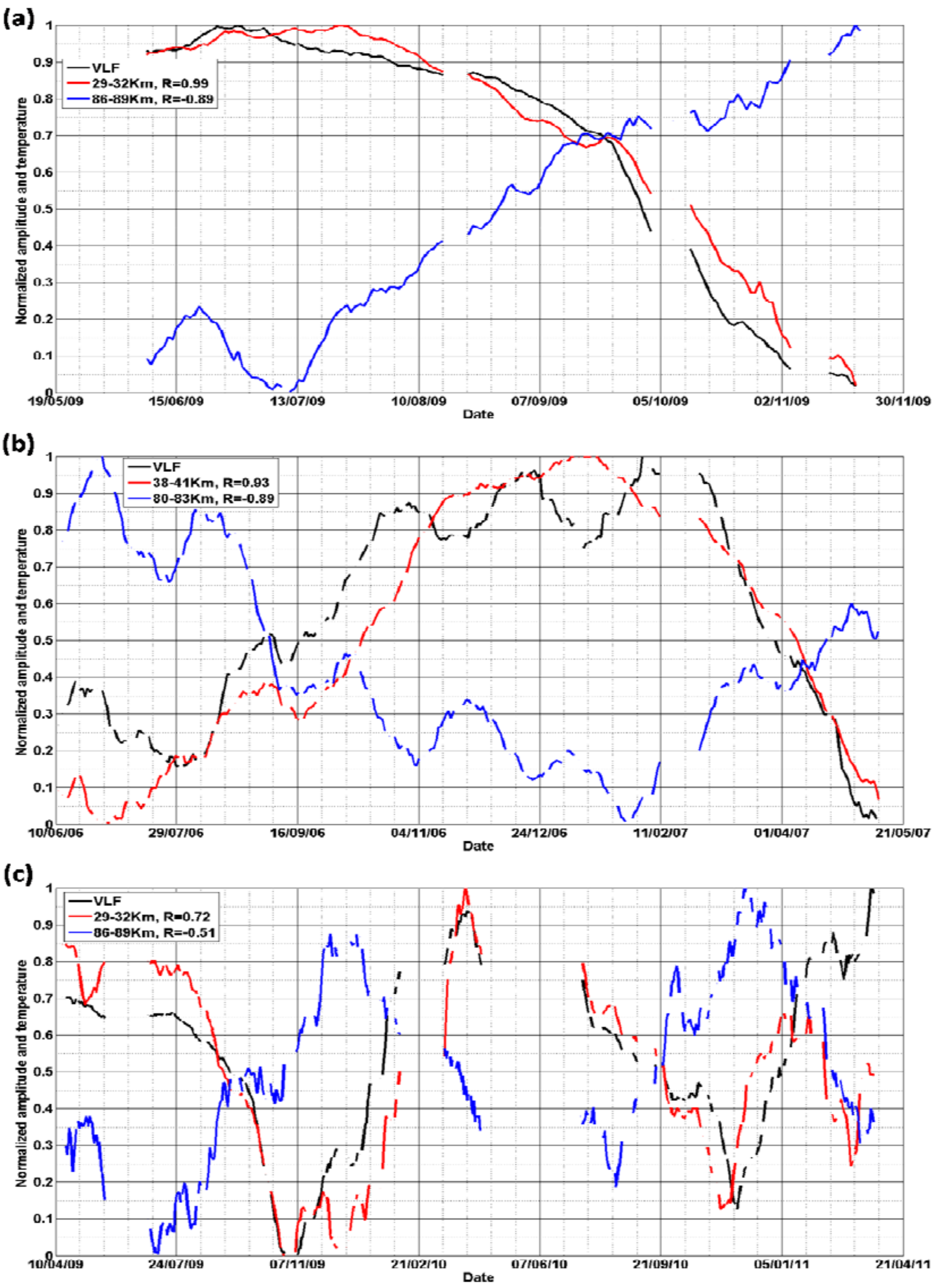

Figure 4: 20-days-running-average of normalized VLF amplitude (black) and normalized temperature values of the layers with maximum positive (red) and negative (blue) correlations with the VLF data, for (a) SB-DHO 2009, (b) DN-NWC 2006-2007 and (c) MH-NSC 2009-2011 data sets. Correlation coefficients values are given in the legend boxes. The gaps imply lack of VLF data.

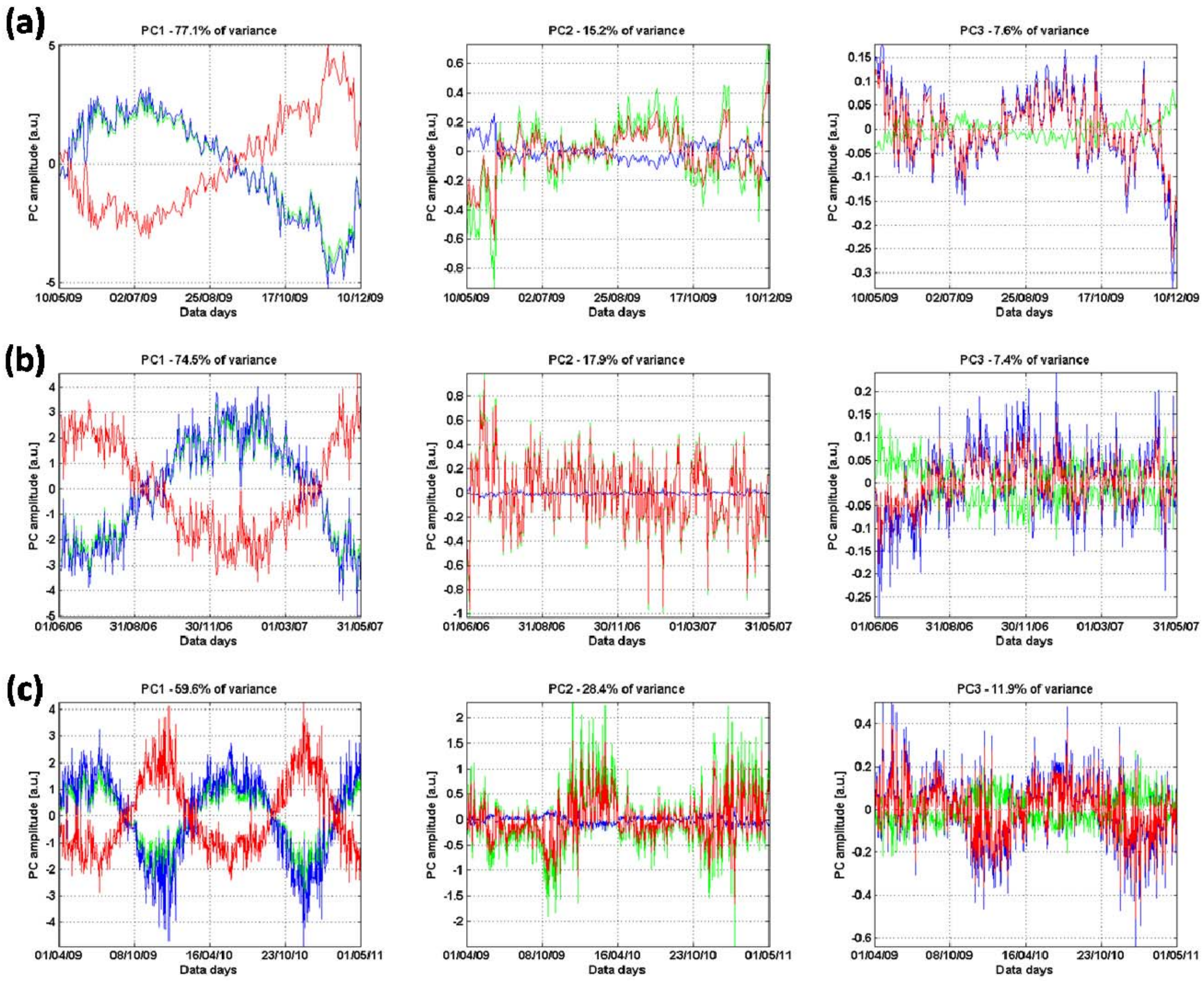

Figure 5: PC (1-3) time series for (a) SB-DHO 2009, (b) DN-NWC 2006-2007 and (c) MH-NSC 2009-2011 data sets, multiplied by the PC coefficients of the VLF data (solid green line), solar irradiance (solid blue line), and 80-90 km average temperature (solid red line). The explained variance of each PC is written above each window.

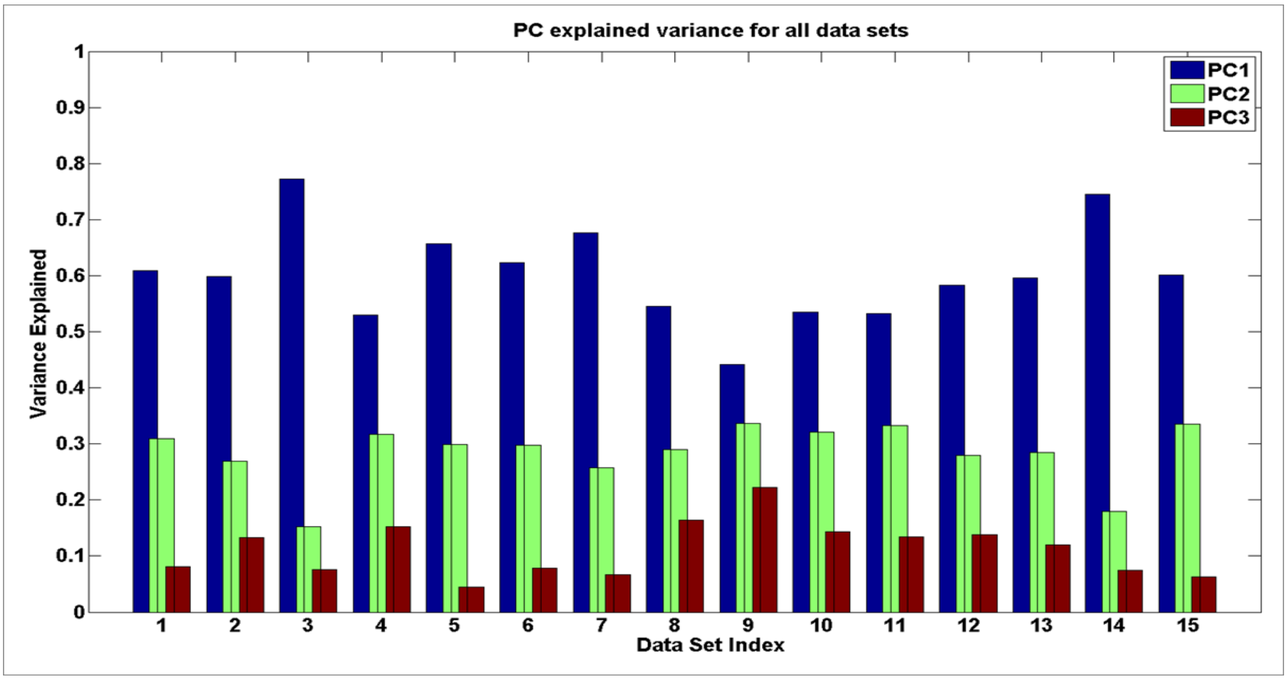

Figure 6: PCA explained variance for all data sets. Indices for the data sets numbers are shown in Table 2.

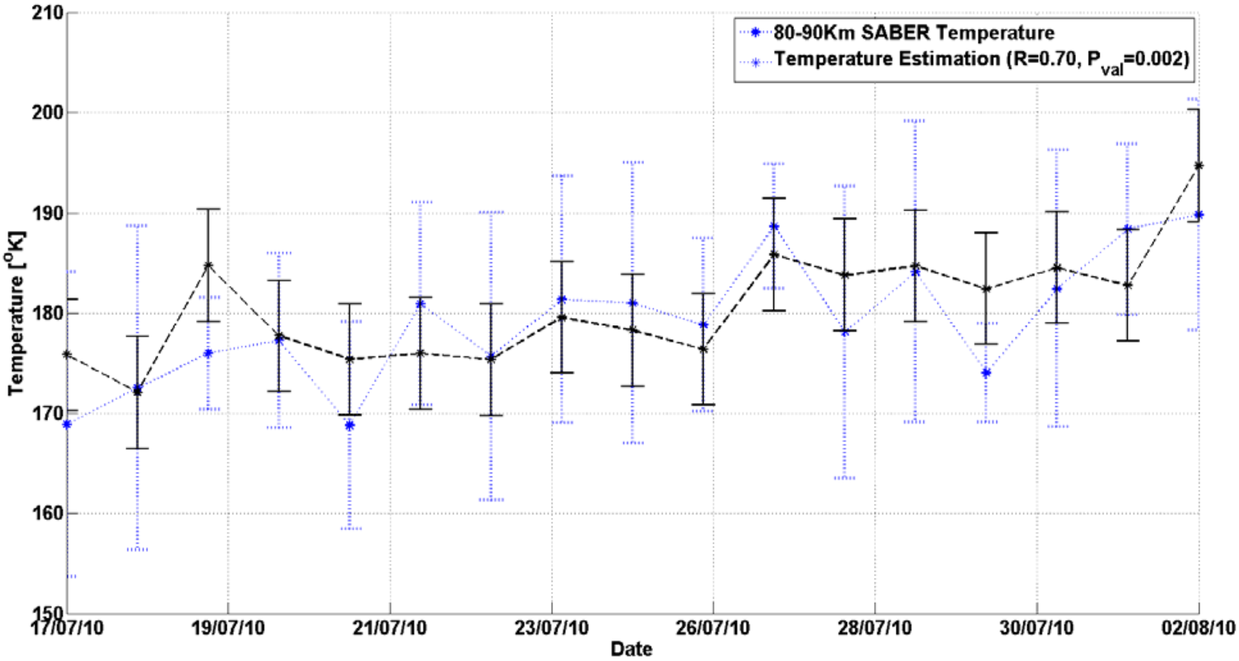

Figure 7: Temperature estimation (dashed black) and SABER temperature (solid blue) time series for SB-DHO 2010 data set. The Pearson's correlation coefficient and P_{val} are written in the legend box.

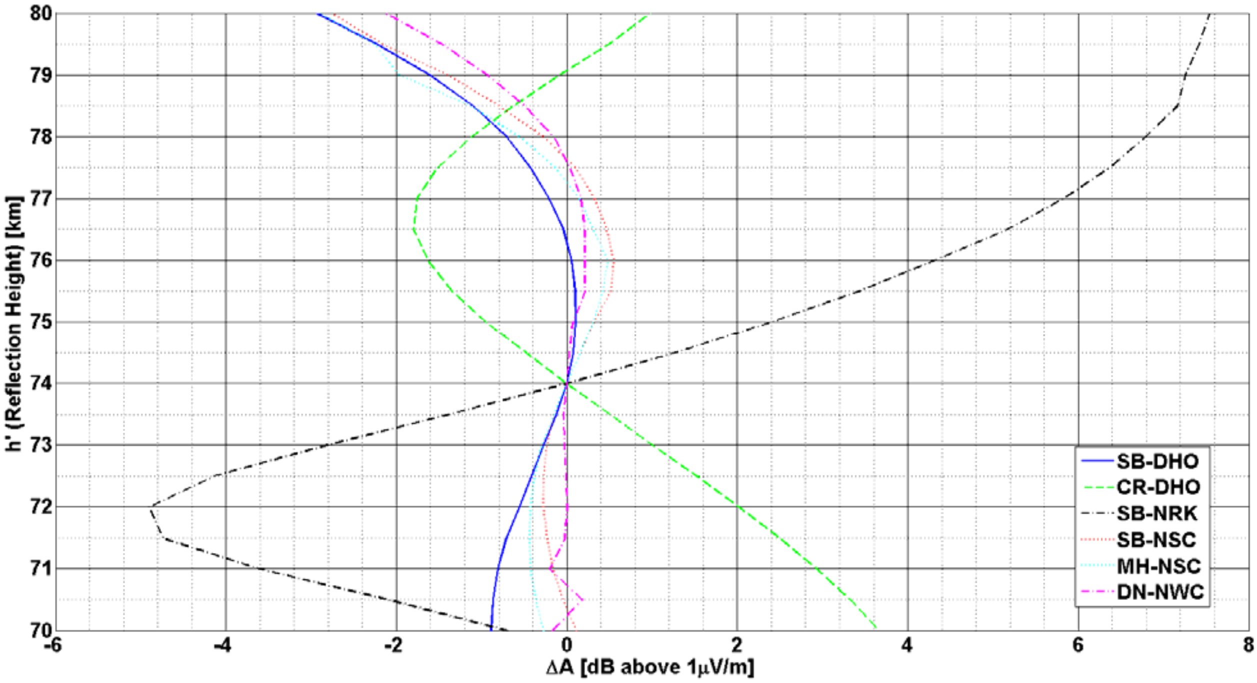

Figure 8: LWPC model results showing the received amplitude change (in dB units) as a function of reflection height displacement from the typical daytime ionospheric values of β=0.3 km^{-1} and h'=74 km, for the GCPs which were examined in this study.